Nuclear Engineering and Design 310 (2016) 656–663

Contents lists available at ScienceDirect

Nuclear Engineering and Design

journal homepage: www.elsevier.com/locate/nucengdes

One-dimensional two-fluid model for wavy flow beyond the Kelvin–Helmholtz instability: Limit cycles and chaos

Martín Lopez de Bertodano [a,*], William D. Fullmer [b], Alejandro Clausse [c]

[a] School of Nuclear Engineering, Purdue University, West Lafayette, IN 47907, USA
[b] Department of Chemical and Biological Engineering, U. of Colorado, Boulder, CO 80309, USA
[c] CNEA-CONICET and Universidad Nacional del Centro, 7000 Tandil, Argentina

ARTICLE INFO

Article history:
Received 17 May 2016
Accepted 21 May 2016
Available online 25 June 2016

JEL classification:
A-Engineering Mechanics

ABSTRACT

A 1D TFM numerical simulation of near horizontal stratified two-phase flow is performed where the TFM, including surface tension and viscous stresses, is simplified to a two-equation model using the fixed-flux approximation. As the angle of inclination of the channel increases so does the driving body force, so the flow becomes KH unstable, and waves grow and develop nonlinearities. It is shown that these waves grow until they reach a limit cycle due to viscous dissipation at wave fronts. Upon further inclination of the channel, chaos is observed. The appearance of chaos in a 1D TFM implies a nonlinear process that transfers energy intermittently from long wavelengths where energy is produced to short wavelengths where energy is dissipated by viscosity, so that an averaged energy equilibrium in frequency space is attained. This is comparable to the well-known turbulent stability mechanism of the multi-dimensional Navier–Stokes equations, i.e., chaos implies Lyapunov stability, but in this case it is strictly a two-phase phenomenon.

1. Introduction

It is well known that the one-dimensional two-fluid model (1D TFM) may be rendered well-posed once appropriate short wavelength physics is incorporated. For example the surface tension force makes the TFM well-posed for horizontal stratified flows beyond the Kelvin–Helmholtz (KH) instability (Ramshaw and Trapp, 1978). This is a proper physical solution to the linear stability problem, but the finite exponential wave growth remains. However, the TFM is inherently non-linear, and little is known about its non-linear stability. The purpose of this paper is to investigate the Lyapunov stability of a 1D TFM beyond the KH criterion.

The state-of-the-art of the 1D TFM stability analysis remains more or less where it was when the present generation of US TFM nuclear reactor safety codes were written in the early seventies, that is, within the realm of linear stability theory. Later advances in the field of non-linear dynamics and chaos have not transcended yet into the understanding of the stability of the TFM.

In the first place Whitham (1974) elaborated a set on non-linear solutions to the two-equation shallow-water theory (SWT) consisting of shocks and expansion waves and identified the kinematic SWT instability. But SWT differs from TFM in one important aspect: it does not include the dynamic KH instability. Beyond that, Kreiss and Ystrom (2002) (KY) analysed a two-equation model that is dynamically similar to the TFM beyond the KH instability. They obtained shocks and expansion waves similar to SWT and observed that the viscous force limits the growth of the waves. Furthermore, Fullmer et al. (2014a) showed that the KY equations are chaotic.

Recently Lopez de Bertodano et al. (2013) derived the two-equation fixed-flux model from the TFM that reduces exactly to SWT for flow conditions below the KH instability, thus rendering the TFM amenable to Whitham's analyses. The fixed-flux model is based on the fixed flux assumption, which allows local instabilities like SWT and KH, but precludes global instabilities like flow excursion and density waves. In this paper the fixed-flux model is applied to perform a stability assessment of Thorpe's experiment (Thorpe 1969) beyond the initial wave growth period, including linear analysis and nonlinear simulations, resulting in limit cycles and chaos.

2. Fixed-flux two-equation model

The incompressible fixed-flux TFM of Lopez de Bertodano et al. (2013) obtained from the full TFM of Fullmer et al. (2014b) and validated with the experiment of Thorpe (1969) is given by:

* Corresponding author.
E-mail address: bertodan@purdue.edu (M. Lopez de Bertodano).

http://dx.doi.org/10.1016/j.nucengdes.2016.05.038
0029-5493/

Nomenclature

c	wave speed (m s^{-1})
C	coefficient of void gradient term in momentum equation (m^2 s^{-2})
$C(r)$	number of points of a trajectory contained in hypersphere of radius r
f	friction factor
g	acceleration due to gravity (m s^{-2})
H	channel height (m)
j	volumetric flux (m s^{-1})
k	wave number (m^{-1})
L	test section length (m)
r	radius
r_ρ	density ratio
u	velocity (m s^{-1})

Greek letters

α	volume fraction
λ	wavelength (m)
μ	dynamic viscosity (Pa s)
ν	kinematic viscosity (m^2 s^{-1})
ρ	density (kg m^{-3})
σ	surface tension (N m^{-1})
θ	angle of channel inclination (rad)
ω	angular frequency (s^{-1})

Subscripts

1	heavier phase
2	lighter phase
i	interfacial
ρ	density ratio

Acronyms

KH	Kelvin–Helmholtz
SWT	shallow water theory
TFM	two-fluid model
1D	one dimensional

$$\frac{\partial \alpha_1}{\partial t} + u_1 \frac{\partial \alpha_1}{\partial x} + \alpha_1 \frac{\partial u_1}{\partial x} = 0, \tag{1}$$

$$\frac{\partial u_1}{\partial t} + \frac{1-\alpha_1}{1-\alpha_1+\alpha_1 r_\rho}\left(u_1 + r_\rho \frac{\alpha_1}{1-\alpha_1}(2u_2 - u_1)\right)\frac{\partial u_1}{\partial x} - \frac{1-\alpha_1}{1-\alpha_1+\alpha_1 r_\rho} C \frac{\partial \alpha_1}{\partial x} = \frac{1-\alpha_1}{1-\alpha_1+\alpha_1 r_\rho}\left(\frac{\sigma H}{\rho_1}\frac{\partial^3 \alpha_1}{\partial x^3} + F_{visc} + F\right), \tag{2}$$

where,

$$C = \left[r_\rho \frac{(u_2-u_1)^2}{1-\alpha_1} - (1-r_\rho r) g_y H\right] \tag{3}$$

is the void convection coefficient and the algebraic drag terms are grouped as

$$F = g_x - \frac{1}{\alpha_1 H}\frac{f_1}{2}|u_1|u_1 + \frac{1}{\alpha_2 H}\frac{f_2}{2} r_\rho |u_2|u_2 + \left(\frac{1}{\alpha_1 H} + \frac{1}{\alpha_2 H}\right)\frac{f_i}{2} r_\rho |u_2 - u_1|(u_2 - u_1). \tag{4}$$

Finally, it can be shown that the combined viscous force, assuming the viscosity is the same for both phases, is:

$$F_{visc} = \nu\left[\left(\frac{1}{\alpha_1} + \frac{r_\rho}{\alpha_2}\right)\frac{\partial}{\partial x}\alpha_1 \frac{\partial u_1}{\partial x} + \frac{r_\rho}{\alpha_2}\frac{\partial}{\partial x}\frac{u_1}{\alpha_2}\frac{\partial \alpha_1}{\partial x}\right]. \tag{5}$$

Two more equations are needed for closure. The first is the void fraction restriction

$$\alpha_1 + \alpha_2 = 1. \tag{6}$$

Secondly we consider the total flux to express the velocity of one component in terms of the other. By combining the time derivative of Eq. (6) with the sum of the phasic continuity equations one gets:

$$\frac{\partial}{\partial t}(\alpha_1 + \alpha_2) + \frac{\partial}{\partial x}(\alpha_1 u_1 + \alpha_2 u_2) = \frac{\partial j}{\partial x} = 0 \tag{7}$$

where j is the total volume flux.

Eq. (7) shows that, provided that the phase densities are constant, j is spatially uniform, i.e., $j(x,t) = j(t)$. For the present case of Thorpe (1969), stagnated flux restriction applies, i.e., $j(t) = 0$. This key assumption greatly simplifies the TFM equations without removing the local material instabilities.

If C is negative and surface tension is neglected, the two-equation fixed-flux model in the limit $r_\rho \to 0$ becomes the well-known 1D SWT equations (Whitham 1974; Wallis 1969). Furthermore $C = 0$ leads to the long wavelength Kelvin–Helmholtz criterion, e.g., see Eq. (2–147) of Ishii and Hibiki (2006),

$$(u_2 - u_1)^2 > \frac{1-r_\rho}{r_\rho}(1-\alpha_1) g_y H \tag{8}$$

If C is positive the equations represent the Kelvin–Helmholtz unstable regime which is the case of the TFM, beyond the scope of SWT, under study. We are now in a position to define the types of waves and instabilities that will be analysed.

The dynamic wave speed, derived later, is given by $c = \sqrt{-\alpha_1 C}$ and the corresponding instability condition is $C > 0$, associated with the dynamic KH instability. On grounds of the analogy between the TFM and SWT, it may be stated that the linear and non-linear behaviour of the dynamically stable TFM (i.e., $C < 0$) may be understood in terms of the many well-known results derived in SWT. If $C = 0$ and $F = 0$ the system becomes the water faucet model of Ransom (1984) which is of practical interest to the verification of the TFM for nuclear reactor safety codes. The case $C > 0$ corresponds to the dynamically unstable incompressible TFM, and it is of unique interest to two-phase flow analysis in general and reactor safety codes in particular, because it is ill-posed when surface tension is not included. However, the nonlinear behaviour of the well-posed case has not been explored beyond the pioneering mathematical analyses of Kreiss and Ystrom (2002) and Keyfitz et al. (2004).

2.1. Viscous term

Additional constitutive equations are required for the closure of the wall and interfacial shear terms and the effective viscosities. For the present calculations the values are $f_1 = f_2 = 0.005$, and $f_i = 0.014$. More importantly, the effective viscosity needs to be specified. Alas, a complete model for the turbulent viscosity is not presently available. In its stead, a rough, order-of-magnitude model is proposed here, which hopefully suffices for the numerical simulations. Since the densities of the Thorpe experiment (1969) are quite close, a first-order approximation is to neglect the

damping action of the interface and treat the two-fluid flow as a single-phase temporal mixing layer. By assuming the mixing layer is self-semilar (i.e., the space–time dependence can be collapsed into a single dependent variable), the turbulent viscosity can be derived analytically (Pope 2000),

$$\nu_T = 0.39^2 S\ \delta(t)\Delta U, \tag{9}$$

where S is the spreading rate, $\delta(t)$ is the mixing layer thickness and ΔU is the absolute value of the velocity difference between the two streams. Due to the self-similar assumption, Eq. (9) is only valid if $S \equiv \frac{1}{U}\frac{d\delta}{dt}$ is a constant. A constant spreading rate has been verified experimentally and via direct numerical simulation for single phase flows with reported values ranging from S from 0.06 to 0.11 (Pope 2000). In the present case of the Thorpe experiment, the velocities of both "streams" – and hence their difference – increase linearly in time, so that Eq. (9) holds only if the mixing layer thickness expands quadratically in time. A VOF-LES simulation of the experiment of Thorpe performed previously by Fullmer et al. (2011) was used to verify that this is approximately the case for $S \approx 0.0137$ to 0.0252. Here, we take the mean value of this range so that $S \approx 0.02$. Finally, rather than using a time dependent mixing layer thickness, the maximum value is taken, i.e., $\delta(t) \approx H$. This results in the following very simple turbulent viscosity model, which is used for all the numerical simulations,

$$\nu_T = 0.003H|u_2 - u_1|. \tag{10}$$

For the present case results $\nu_T = 0.000025\,\frac{m^2}{s}$.

3. Thorpe experiment

The conditions and properties of the Thorpe experiment (1969) for near horizontal stratified wavy flow, shown in Fig. 1, are used for the linear and non-linear stability analyses that follow. The critical wavelength data for the inclination angle $\theta = 0.072$ rad were already used by Fullmer et al. (2014b) to compare with the linear stability analysis. In the experiment, two immiscible liquids, water and a kerosen-carbon-tetrachloride mixture, equally fill a rectangular channel of dimensions 0.03 m tall, 0.1 m wide and 1.83 m long. Since both ends of the channel are closed the flux is simply $j = 0$. The material properties are given in Table 1.Initially the channel is at rest in the horizontal position allowing the fluids to reach uniform stratified equilibrium. Then the channel is suddenly tilted at a small specified angle developing a counter-current flow as the denser water rushes down and pushes the lighter kerosene up. For the case $\sin(\theta) = 0.072$ a series of photographs of the flow viewed from the side were published. The dominant wavelength measured at the onset of wave formation is approximately 3.5 ± 1 cm which is similar to the prediction of the most dangereous wavelength in Fig. 2.

Table 1
Material properties of the Thorpe experiment.

Property	Water	Kerosene
ρ_k (kg/m^3)	1000	780
μ_k (Pa s)	0.001	0.0015
σ_{12} (N/m)	0.04	–

4. Linear stability analysis

We consider the model with $F = 0$ since we are interested in the linear dynamics, which is not influenced by this term. Eqs. (1) and (2) can be written as:

$$\mathbf{A}\frac{\partial}{\partial t}\underline{\phi} + \mathbf{B}\frac{\partial}{\partial x}\underline{\phi} + \mathbf{D}\frac{\partial^2}{\partial x^2}\underline{\phi} + \mathbf{E}'\frac{\partial^3}{\partial x^3}\underline{\phi} = 0 \tag{11}$$

where,

$$\mathbf{B} = \begin{bmatrix} u_1 & \alpha_1 \\ -\frac{1-\alpha_1}{1-\alpha_1+\alpha_1 r_\rho}C & \frac{1-\alpha_1}{1-\alpha_1+\alpha_1 r_\rho}\left(u_1 + r\frac{\alpha_1}{1-\alpha_1}(2u_2 - u_1)\right) \end{bmatrix},$$
$$\mathbf{D} = \begin{bmatrix} 0 & 0 \\ 0 & -\frac{1-\alpha_1}{1-\alpha_1+\alpha_1 r_\rho}\nu \end{bmatrix}, \tag{12}$$
$$\mathbf{E}' = \begin{bmatrix} 0 & 0 \\ -\frac{1-\alpha_1}{1-\alpha_1+\alpha_1 r_\rho}\frac{\sigma H}{\rho_1} & 0 \end{bmatrix}.$$

The characteristics, given by the condition $Det[\mathbf{B} - \lambda\mathbf{A}] = 0$ describe the behaviour of the first order system, namely:

$C < 0$: $c = u_1 \pm \sqrt{|C|\alpha_1}$, two real roots, $C = 0$: $c = u_1$, one real root, $C > 0$: $c = u_1 \pm i\sqrt{|C|\alpha_1}$, two imaginary roots.

The first two cases are well-posed and well-understood. However the last case leads to difficulties and will be analysed in detail using a dispersion analysis.

The dispersion relation extends the results of the characteristic analysis to the full spectrum of wavelengths and it incorporates the effects of viscosity and surface tension. The first step is to linearize the two equation system using $\underline{\phi} = \underline{\phi}_0 + \underline{\phi}'$. Then a Fourier solution, $\underline{\phi}' = \underline{\hat{\phi}}' e^{i(kx-\omega t)}$, is inserted into the linearized equations, where k and ω are the wave number and the angular frequency. From linear theory, the condition necessary for a non-trivial solution is:

$$Det[-i\omega\mathbf{A} + ik\mathbf{B} + (ik)^2\mathbf{D} + (ik)^3\mathbf{E}'] = 0 \tag{13}$$

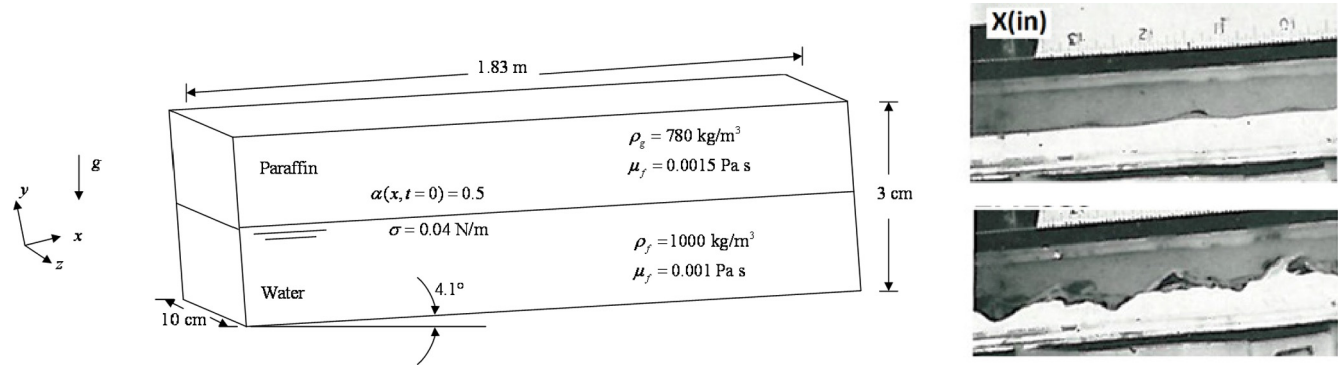

Fig. 1. Thorpe experiment schematic (left). Experimental photographs (right) at 2.06 and 2.35 s. [Photographs reprinted from Thorpe (1969) with permission from Cambridge University Press.].

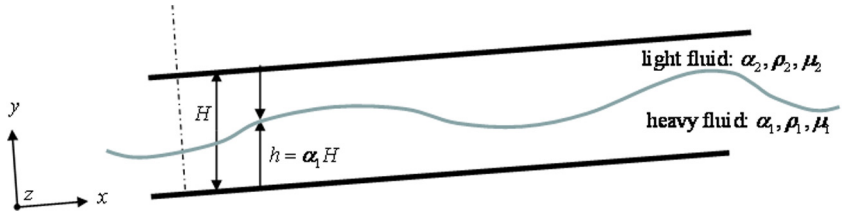

Fig. 2. Near horizontal wavy flow schematic.

4.1. Stable regime

The stable model (i.e., $C \leqslant 0$) corresponds to gas velocities below the KH limit. In the limit of infinitesimal wavelengths, i.e., $k \to \infty$, the wave velocities are the characteristic speeds, which are real and therefore the stable model is hyperbolic. Hyperbolicity is a characteristic feature of well-posed linearly-stable wave propagation models. Stable waves do not grow in time and only propagate at the characteristic speed. The inviscid case without surface tension becomes the well-known SWT in the limit $r_\rho \to 0$ (Whitham, 1974).

While the linear stability characteristics are very simple, the non-linear behaviour is not so simple and leads to material shocks equivalent to those encountered in the Burgers' equation. The dispersion relation for finite wavelengths retain this characteristic behavior, but the effects of viscosity and surface tension make the system dissipative (i.e., the wave amplitude decreases with time) and dispersive (i.e., different wavelengths travel at different speeds).

4.2. Unstable regime

The fixed-flux TFM departs from single-phase SWT once it turns dynamically unstable, i.e., once Eq. (8) is satisfied. The dispersion analyses including the effective viscosity given by Eq. (10), the kinematic viscosity and surface tension, was performed with Thorpe'sconditions, namely: $H = 0.03$ m, $\alpha = 0.5$, $u_1 = -u_2 = 0.2$ m/s, $r_\rho = 0.78$, $\nu = 0.000025$ m^2/s and $\sigma H/\rho_1 = 1.2\times 10^{-6}$ m^4/s^2. The results are shown in Fig. 2. The first significant outcome is the fast wave growth rate for all cases, which is brought about by the KH instability.

The basic, or fundamental, 1D TFM dispersion relation is obtained from the solution of Eq. (13) with $\varepsilon = \nu = 0$ and $\sigma = 0$. Beyond the KH limit this model is ill-posed, i.e., growth rates increase unboundedly as the wavelength shrinks to zero. The zero wavelength growth rate is infinite for any relative velocity except for the trivial case of homogeneous flow, i.e., zero relative velocity. This is the well-known ill-posed TFM (Lyczkowski et al., 1978). Furthermore, when wall and interfacial friction are included, even with unrealistically large coefficients values, they do not change the ill-posed nature of the dynamic instability at the zero wavelength. In turn, adding kinematic viscosity, $\nu = 0.000025$ m^2/s, makes the model technically well-posed since the growth rate becomes finite at zero wavelength. However the growth rate is still maximum and very high there, i.e., $\omega_i = \frac{\alpha_1 C}{\nu}$, which is similarly unphysical (Arai 1980). While this model is not strictly ill-posed, it is practically so.

On the other hand, Fig. 3 shows that surface tension makes the model well-posed with the advantage that it is more realistic. The cut-off wavelength corresponding to the surface tension of water-kerosene, $\sigma = 0.04$ N/m, is approximately 20 mm. Furthermore the most dangerous wavelength matches approximately the experimental measurement of 35 mm. This confirms that, for Thorpe's experiment, the KH instability is indeed the appropriate mechanism. The figure also shows that the effect of viscosity on the linear stability is negligible compared to surface tension. Surface tension regularization (Ramshaw and Trapp 1978) is the earliest published demonstration that the TFM may be rendered well-posed for unstable flow by including appropriate short wavelength physics. Nevertheless, even when the model is well-posed, there is still a strong exponential wave growth which presents challenges to practical applications of the 1D TFM. In the next section a nonlinear analysis is presented that overcomes this difficulty. It will be shown that, while surface tension is the key mechanism of linear stability, viscosity is the key mechanism of non-linear stability.

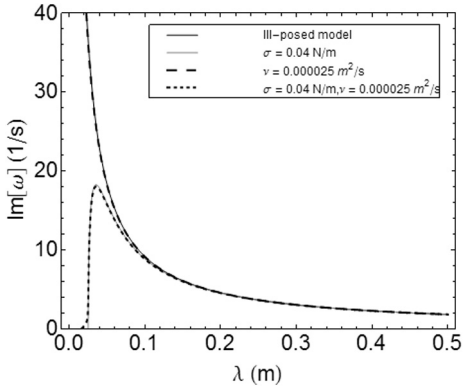

Fig. 3. Dispersion relation for Thorpe experiment.

5. Numerical simulations

In this section the nonlinear behaviour of the TFM is performed by numerical simulations. The 1D model of Eqs. (1)–(7) is solved numerically with the second order numerical method proposed by Fullmer et al. (2014a). The primary objective of the non-linear analysis is to understand how a model that is linearly unstable is nevertheless bounded in the long term. Barnea and Taitel (1994) have shown that, in general, when the governing model is linearly unstable, perturbations grow and cut-off and critical wavelengths are generally consistent with linear theory. The typical initial non-linear behavior is for waves to steepen into Burgers-like shocks (Whitham 1974). Furthermore, Kreiss and Ystrom (2002) have demonstrated that the waves stop growing because of the interaction of viscosity and the material shocks. Here, we seek to understand what happens as $t \to \infty$.

Unfortunately, the time and space constraints of the Thorpe experiment make it impossible to do such a calculation for that particular test section. Therefore, in order to run a simulation for a longer period of time, a problem is proposed to reproduce the conditions in the center of the channel but in an infinite domain, i.e., with periodic boundary conditions instead of the closed ends. An angle of inclination greater than $\theta = 0.027$ rad is required for the KH critical velocity given by Eq. (8). The length of the computational domain is $L = 1$ m. It was found that starting the simula-

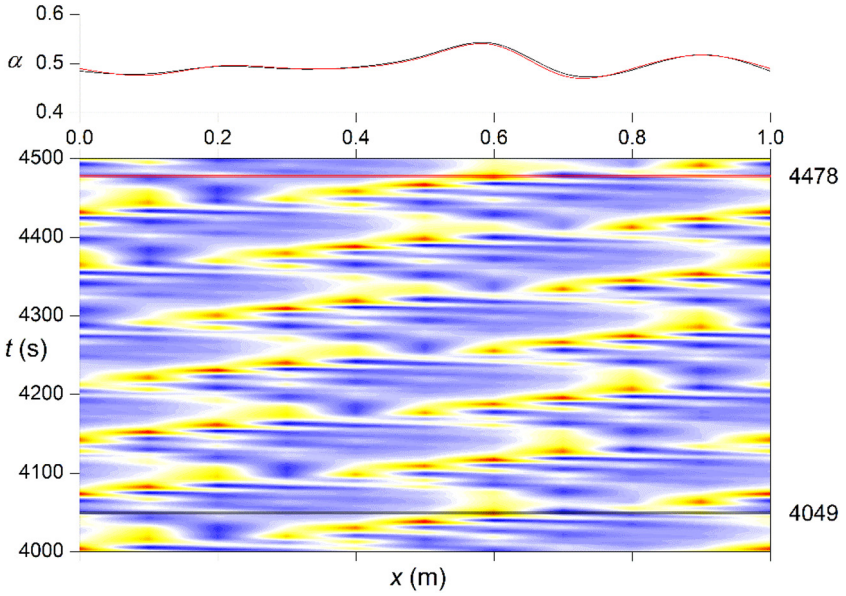

Fig. 4. Color map of $\alpha(x,t)$ for $\theta = 0.0276$ (periodic). The crossing horizontal lines (red and black) indicate the position of the profiles depicted in top margin at times 4049 and 4478 s. (For interpretation of the references to colour in this figure legend, the reader is referred to the web version of this article.)

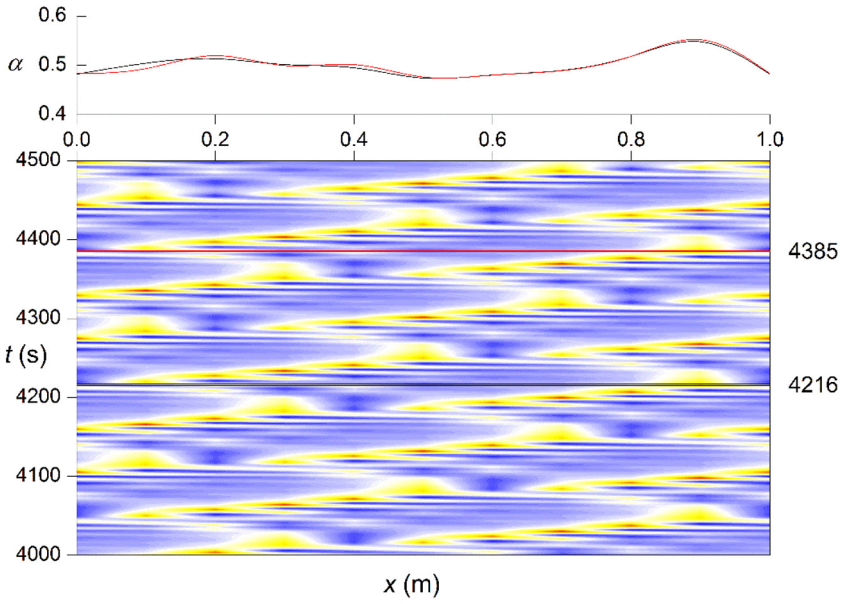

Fig. 5. Color map of $\alpha(x,t)$ for $\theta = 0.0277$ (periodic). The crossing horizontal lines (red and black) indicate the position of the profiles depicted in top margin at times 4216 and 4385 s. (For interpretation of the references to colour in this figure legend, the reader is referred to the web version of this article.)

tions from the kinematic condition, i.e., $F = 0$ in Eq. (4), with an initial perturbation in the void fraction minimizes unnecessary transients. Then the initial condition is $\alpha_1 = 0.5 + 0.02e^{\left(\frac{x-x_0}{0.01}\right)^2}$ and the velocity is set by the kinematic condition.

To keep the flows from being brought to rest under the shear dissipation, a constant, uniform source must be added. In the physical case, the axial component of gravity acts in the same direction for both fluids and if it were not for the closed ends, both fluids would accelerate downward and reach larger phasic velocities than in the countercurrent case. To keep the flow countercurrent, a horizontal hydrostatic force (x-direction) is added to each phase that is equal and opposite. The corresponding source term for Eq. (4) is $F_h = (1 - r)g \sin\theta$.

We present results for the narrow range of inclinations where the flow turns from limit cycle to chaotic. Figs. 4 and 5 show the maps of $\alpha(x,t)$ in color scale for $\theta = 0.0276$ and 0.0277. In both cases the solution is periodic, which is revealed by the repetition of the void-fraction profile (top margin plot) taken at 4049 and 4478 s in the first case (period ~429 s) and at 4216 and 4385 s in the second case (period ~169 s). On the other hand, for $\theta = 0.028$, Fig. 6, the map shows the rupture of the periodicity leading to aperiodic chaotic behavior where the regularity of the standing wave is lost, i.e., uniform amplitudes, periods, propagation speeds, etc, are no longer observable. This may also be seen the Fourier transforms of the solutions for $\theta = 0.0276$ and 0.028, shown in Figs. 7 and 8 respectively. In the limit cycle right before chaos the discrete

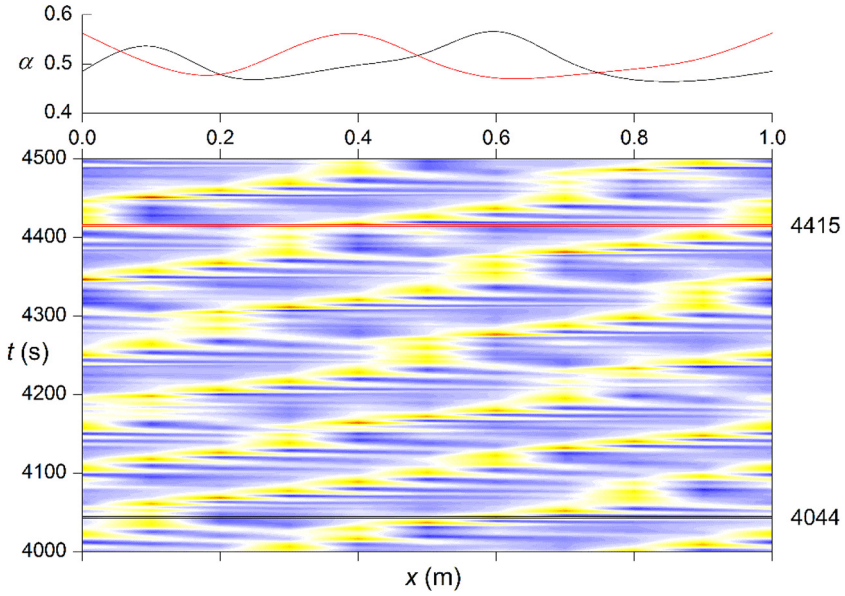

Fig. 6. Color map of $\alpha(x,t)$ for $\theta = 0.028$ (aperiodic). The crossing horizontal lines (red and black) indicate the position of the profiles depicted in top margin at times 4044 and 4415 s. (For interpretation of the references to colour in this figure legend, the reader is referred to the web version of this article.)

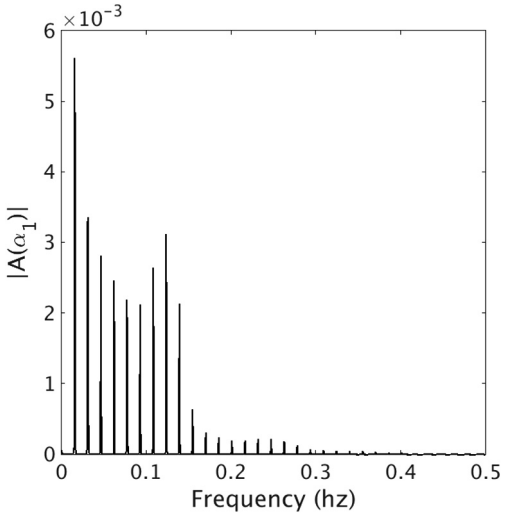

Fig. 7. Fourier transform of limit cycle, $\theta = 0.0277$.

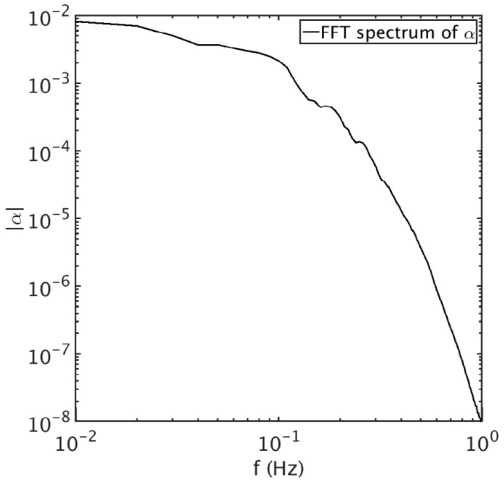

Fig. 8. Fourier transform of chaos, $\theta = 0.028$.

frequency components of the solution are clear, whereas once chaos breaks out the spectrum becomes continuous.

The continuous spectrum of Fig. 8 is of particular interest because it implies a new non-linear bounding mechanism. The chaotic formation of steep wave fronts and expansion at the back of the waves needs to be analyzed further, but it resembles 2D turbulence in the sense that energy is transferred to short and long wavelengths. What is different is that there is a net nonlinear energy transport to short length scales, i.e., the wave fronts, where it is dissipated by viscosity and, in this sense, it resembles 3D turbulence.

Two standard non-linear stability tests were performed in addition to the Fourier spectrum to characterize the chaotic behavior at $\theta = 0.028$. The first test is the calculation of the largest Lyapunov exponent (ω_{LLE}) (Sprott 2003), which is the nonlinear counterpart of the linear growth rate obtained from the dispersion analysis shown in Fig. 3. More specifically, ω_{LLE} indicates the average rate at which two nearby states converge to, or diverge from, one another. For discretized time, ω_{LLE} can be assessed as:

$$\omega_{LLE} = \sum_{t=0}^{t\to\infty} \frac{1}{\Delta t} \ln \frac{\delta(t)}{\delta_0} \tag{14}$$

where δ_0 is a small initial separation between two trajectories (solutions) and $\delta(t)$ is the corresponding separation at a later time t. A positive ω_{LLE} indicates that the solutions are diverging and that the system is chaotic, and its magnitude approximates the rate at which the predictability of the system is lost. Fig. 9 shows the absolute value of the difference between a state evolving in the limit cycle for $\theta = 0.0277$ and two evolutions starting close to the cycle. The rate of convergence, i.e., the LLE, is $-0.04 \pm 0.01\ s^{-1}$. Once the trajectories merge in the limit cycle, the separation remains oscillating around a constant value given by the shift in the direction of the phase-space flow. Along that direction the Lyapunov exponent is zero. On the other and, Fig. 10 shows the divergence of several solutions for $\theta = 0.028$ with slightly perturbed initial conditions compared to the unperturbed case. The corresponding estimation of ω_{LLE} resulted $0.07 \pm 0.01\ s^{-1}$. This may be compared with the maximum linear growth rate from Fig. 3 and $18\ s^{-1}$, which is two orders of magnitude grater. Hence, the chaotic wavy solution is signifi-

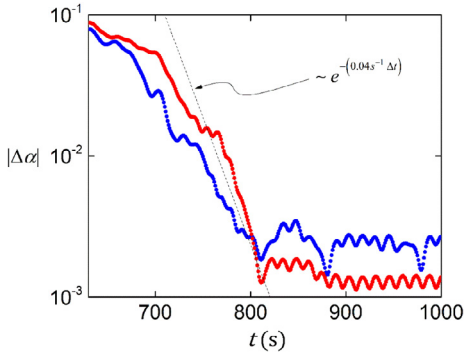

Fig. 9. Absolute value of the difference between the limit cycle solution for $\theta = 0.0277$ and two evolutions starting close to the cycle. $|\Delta\alpha|$ is the L_2 norm taken over 16 fixed equidistant positions.

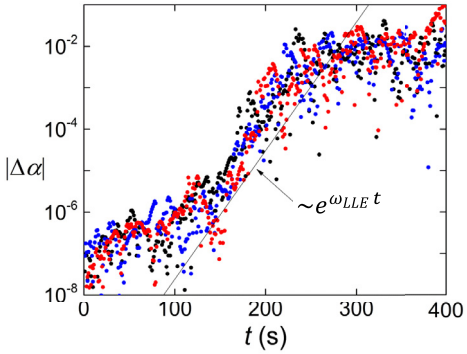

Fig. 10. Absolute value of the difference between three pairs of chaotic solutions ($\theta = 0.028$) starting with slightly perturbed initial conditions for $|\Delta\alpha|$ is the L_2 norm taken over 16 fixed equidistant positions.

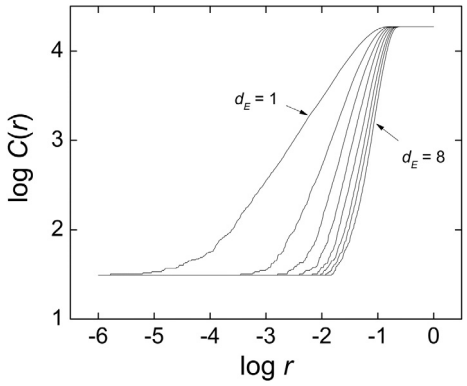

Fig. 11. Number of points of a trajectory for for $\theta = 0.028$, $C(r)$, contained in a d_E-dimensional ball of radius r. The slope of the midsection in logarithmic scale is the fractal correlation dimension.

cantly more stable than the smooth initial condition, which allows the model to become bounded. This is the reason why linear analysis is misleading and nonlinear analysis is necessary to understand that a Lyapunov stable TFM is imaginable.

Another important characteristic test of chaos is the fractal dimension of the phase-space dynamics, which measures the "strangeness" of the attractor (Grassberger and Procaccia 1983; Ruelle 1989; Manneville 2010). In the present case, the fractal correlation dimension d_c was used for its simplicity (Abarbanel 1996). It is calculated by shrinking a d_E-dimensional hypersphere of

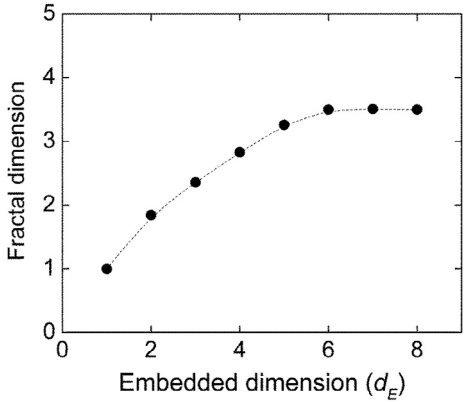

Fig. 12. Dependence of the fractal correlation dimension d_F on the embedded dimension d_E ($\theta = 0.028$).

radius r and counting the number of points inside the hypersphere, $C(r)$. As r tends to zero $C(r)$ behaves as

$$C(r) \propto r^{d_c} \tag{15}$$

Therefore, on a logarithmic plot, the slope of $C(r)$ versus r gives the correlation dimension d_c. The difficulty is that there are simultaneously two unknowns: the fractal dimension d_c and the phase-space dimension in which the fractal dimension should be calculated, called the embedded dimension, d_E. In system dynamics each dimension is associated with a state variable, like void fraction in our case. Since the spatial coordinate is continuous, the dimensionality of our problem is actually infinite; but we are assuming that it can be fairly represented by discretizing the space in N segments, leaving a $2N$ dimension system (N for each state field, α and u). However, it may not be necessary to use all $2N$ variables to capture the dynamics of the problem. Therefore, the correlation dimension is first calculated with an embedded dimension of one, which is almost surely insufficient, and then repeated several times, each time increasing the embedded dimension. At some point, the correlation dimension will stop changing, giving both the fractal and the minimum embedded dimension. Fig. 11 shows $C(r)$ in logarithmic scale for d_E from one to eight, taking the void fraction at equidistant positions for $\theta = 0.028$. The successive slopes correspond to d_c, which are plotted on Fig. 12 as a function of d_E. The correlation dimension saturates at $d_c \approx 3.43$ with a minimum embedded dimension of $d_E = 6$, which indicates that in principle the dynamics of the system may be modeled using only six appropriately defined state variables. The embedded dimension is consistent with previous studies performed using the Kreiss–Ystrom two equation model (Fullmer et al. 2014a).

6. Conclusions

The fixed flux 1D TFM for horizontal or slightly inclined two-phase flow has been used to dynamically simulate stratified wavy flow and its transition from smooth flow. The model is based on the full TFM of Fullmer et al. (2014b) previously validated with the experimental data of Thorpe (1969).

It was shown in Fig. 3 that the model with surface tension is well-posed and the linear stability analysis agrees well with the data for the dominant wavelength. However, linear waves grow exponentially and another mechanism is needed to stop their growth, so the focus turns to nonlinear stability due to viscosity. The path from limit cycles to chaos and the continuous spectrum of the solution are strong indications that the 1D TFM is chaotic.

Furthermore a positive Lyapunov coefficient and the fractal dimension have been obtained as quantitative evidence of chaos. For a narrow range of parameters, it is shown that the dynamics of the infinite domain problem are bounded by the attractor alone, independent of physical limitations, i.e., transitions to regions of single-phase flow which are locally stable. The present results offer the first confirmation of computational 1D TFM chaos, beyond the preliminary demonstrations of Fullmer et al. (2014b).

The chaotic solutions consisting of steep wave fronts and expansion of the back of the waves imply that energy is transferred to short and long wave scales with a net nonlinear transport to short length scales where it is dissipated by viscosity. This is comparable to the well-known turbulent stability mechanism of the multi-dimensional Navier–Stokes equations, i.e., chaos implies Lyapunov stability, but in this case it is strictly a two-phase phenomenon.

The current chaotic results still require experimental confirmation beyond the experimental data of Thorpe.

References

Abarbanel, H.D.I., 1996. Analysis of Observed Chaotic Data. Springer, New York.

Arai, M., 1980. Characteristics and stability analyses for two-phase flow equation systems with viscous terms. Nucl. Sci. Eng. 74, 77–83.

Barnea, D., Taitel, Y., 1994. Non-linear interfacial instability of separated flow. Chem. Eng. Sci. 49, 2341–2349.

Fullmer, W.D., Lopez de Bertodano, M.A., Ransom, V.H., 2011. The Kelvin–Helmholtz instability: comparisons of one- and two-dimensional simulations, NURETH-14.

Fullmer, W.D. et al., 2014a. Analysis of stability, verification and chaos with the Kreiss–Ystrom equations. Appl. Math. Comput. 248, 28–46.

Fullmer, W.D., et al., 2014b. Numerical solution of wavy-stratified fluid-fluid flow with the one-dimensional two-fluid model: stability, boundedness, convergence and chaos, FEDSM2014-22121.

Grassberger, P., Procaccia, I., 1983. Characterization of strange attractors. Phys. Rev. Lett. 50 (5), 346–349.

Ishii, M., Hibiki, T., 2006. Thermo-fluid Dynamics of Two-phase Flow, first ed. Springer, New York.

Keyfitz, B.L., Sever, M., Zhang, F., 2004. Viscous singular shock structure for a non-hyperbolic TFM. Nonlinearity 17, 1731–1747.

Kreiss, H.-O., Ystrom, J., 2002. Parabolic problems which are ill-posed in the zero dissipation limit. Math. Comput. Model. 35, 1271–1295.

Lopez de Bertodano, M. et al., 2013. One-dimensional two equation two-fluid model stability. Multiphase Sci. Technol. 25.

Lyczkowski, R.W., Gidaspow, D., Solbrig, C.W., 1978. Characteristics and stability analyses of transient one-dimensional two-phase flow equations and their finite difference approximations. Nucl. Sci. Eng. 66, 378–396.

Manneville, P., 2010. Instabilities, Chaos and Turbulence. ICP Fluid Mech., Imperial College Press, London, UK.

Pope, S.B., 2000. Turbulent Flows, first ed. Cambridge University Press, New York.

Ramshaw, J.D., Trapp, J.A., 1978. Characteristics, stability and short-wavelength phenomena in two-phase flow equation systems. Nucl. Sci. Eng. 66, 93–102.

Ransom, V.H., 1984. Benchmark numerical tests. In: Hewitt, G.F., Delhay, J.M., Zuber, N. (Eds.), Multiphase Science and Technology. Hemisphere, Washington DC.

Ruelle, D., 1989. Chaotic Evolution and Strange Attractors. Cambridge Univ. Press, Cambridge, UK.

Sprott, J.C., 2003. Chaos and Time Series Analysis. Oxford University Press, Oxford, UK.

Thorpe, J.A., 1969. Experiments on the instability of stratified shear flow: immiscible fluids. J. Mech. 39, 25–48.

Wallis, G.B., 1969. One-dimensional Two-phase Flow. McGraw-Hill, New York, New York.

Whitham, G.B., 1974. Linear and Nonlinear Waves. Wiley, New York, New York.